Chinese Chemical Letters 34 (2023) 107716

Contents lists available at ScienceDirect

Chinese Chemical Letters

journal homepage: www.elsevier.com/locate/cclet

Probing region-resolved heterogeneity of phosphoproteome in human lens by hybrid metal organic frameworks

Huimin Chu[a], Haoyang Zheng[a], Aizhu Miao[c,*], Chunhui Deng[a,b,**], Nianrong Sun[a,*]

[a] Department of Gastroenterology and Hepatology, Zhongshan Hospital, and Department of Chemistry, Fudan University, Shanghai 200032, China
[b] Institue of Metabolism & Integrate Biology (IMIB), Fudan University, Shanghai 200433, China
[c] Department of Ophthalmology, Eye & ENT Hospital of Fudan University, Shanghai 200031, China

ARTICLE INFO

Article history:
Received 7 April 2022
Revised 1 July 2022
Accepted 26 July 2022
Available online 28 July 2022

Keywords:
Phosphoproteome
Human lens
Region resolution
Metal organic framework
Metal oxide affinity chromatography
Immobilized metal affinity chromatography

ABSTRACT

Phosphorylation plays crucial parts in lenticular biological function. Getting knowledge of region-resolved phosphoproteome contributes to better comprehending the pathogenesis. Here, we prepared the hybrid metal organic frameworks (HMOFs) for probing the region-resolved heterogeneity of phosphoproteome in human lens. 1334 phosphosites corresponding to 564 phosphoproteins, 1160 phosphosites corresponding to 316 phosphoproteins and 517 phosphosites corresponding to 205 phosphoproteins were identified in capsule, cortex and nucleus, respectively, providing the relatively extensive distribution mapping of phosphorylation in human lens for the first time. The label-free quantification experiments and principal component analysis presented differential expression of phopshoproteins in three subregions. For instance, α-crystallin, β-crystallin and fibrillin-1 closely associated with cataract and Marfan syndrome showed disparate spatial distribution. The preferential phosphoproteins in capsule, cortex and nucleus were involved in cytoskeleton organization, metabolic process and lens development in camera-type eye, respectively. This work first provided a general overview of region-resolved phosphoproteome of human lens.

Human lens is a lamellar and well-ordered structure, which is comprised of capsule, cortex and nucleus that collaboratively refract light to be focused on the retina, indispensable to human vision [1]. It is well known that crystallin dominates the human lens with a high concentration, having molecular chaperone activity and playing important part in apoptosis regulation, neovascularization, redox process and inflammation [2]. The malfunction and aggregation of crystallin could induce many eye diseases with high risk of vision impairment and even blindness, including glaucoma, uveitis, high myopia, and cataracts, seriously deleterious to life quality of patients [3–5]. However, the detailed pathologies of these diseases are not thoroughly clear [5]. Studies show that phosphorylation plays crucial roles in maintaining the homeostasis of lenticular protein, the abnormal of phosphorylation is closely associated with eye diseases especially cataract, the first cause of blindness [6]. Moreover, even if the same kind of phosphoproteins may function differently in various regions. For example, Gray *et al.* reported that more αB-crystallin, a subunit of α-crystallin that associated with cataract formation [7], located at cortex than nucleus in older lens [8]. Therefore, it is of great implication to analyze phosphoproteins in different regions for disclosing disease pathogenesis. While the comprehensive region-resolved phosphoproteins towards human lens have not been reported.

In mass spectrometry (MS)-based phosphoproteomics, metal oxide affinity chromatography (MOAC) and immobilized metal affinity chromatography (IMAC) are two well-investigated approaches for sample pretreatment [9–13]. Researches have shown that IMAC and MOAC display different preference towards mono- and multi-phosphopeptides, and, as a result, the combination of IMAC and MOAC is regarded as the best way to conduct comprehensive phosphopeptide analysis. Up to date, much efforts have been made on the design of IMAC-MOAC hybrid functional nanomaterials [14,15]. Especially, Wang *et al.* integrated the titania and titanium ions by preparing (3-glycidyloxypropyl) trimethoxysilane and adenosine 5-triphosphate solution (GLYMO-ATP) as a linker to construct an IMAC-MOAC hybrid to implement a comprehensive capture towards mono- and multi-phosphopeptides in human lens of cataract and normal [16]. Compared to unitary MOAC, the IMAC-MOAC hybrid exhibited superior performance. In detail, 658 and

* Corresponding authors.
** Corresponding author at: Department of Gastroenterology and Hepatology, Zhongshan Hospital, and Department of Chemistry, Fudan University, Shanghai 200032, China.
E-mail addresses: miaoaizhu@fudan.edu.cn (A. Miao), chdeng@fudan.edu.cn (C. Deng), sunnianrong@fudan.edu.cn (N. Sun).

https://doi.org/10.1016/j.cclet.2022.07.059
1001-8417/

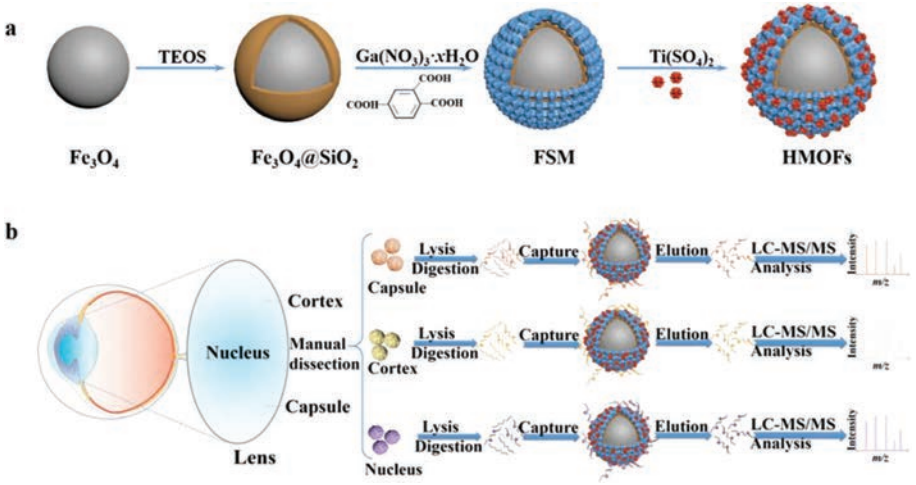

Scheme 1. (a) Workflow of the synthetic procedure of HMOF. (b) Workflow of the identification of phosphopeptides from nucleus, cortex and capsule of human lens.

162 phosphopeptides were identified by IMAC-MOAC hybrids from lens of normal and cataract respectively, whereas only 287 and 68 phosphopeptides were identified by unitary MOAC. These results not only suggested the better and comprehensive capture capacity of IMAC-MOAC hybrid, but also further confirmed the research value of phosphorylation in human lens. Nevertheless, the preparation of this IMAC-MOAC hybrid put forward extremely high requirements for operation, which cannot be broadly adopted. Metal organic frameworks (MOFs) have attracted much attention in phosphoproteomics owing to their facile preparation, abundant metal-oxygen units, large specific surface area, structural tunability and ease of modification [17–22]. In the IMAC-MOAC hybrids, MOFs behaved as MOAC substrates for anchoring of metal ions [23,24], for which different chelating ligands, like glyphosine and phytic acid, were normally demanded because of the lack of free chelate groups in MOFs. For instance, Zhou *et al.* used ATP as chelating ligand to connect the UiO-66-NH_2 with titanium ions [18]. Additionally, Peng *et al.* immobilized zirconium ion on zirconium-organic framework through the reaction of phosphorus oxychloride and 2,4,6-collidine [25]. Although a certain achievement was attained, the additional chemicals inevitably exacerbate the complicacy of synthetic process. Herein, we proposed a new MOF with free carboxyl groups that can be employed to directly immobilize metal ions. The hybrid metal organic frameworks (HMOFs) were attained through a simple assembly strategy without utilization of extra ligands, and applied for region-resolved phosphoproteomics analysis of human crystalline lens. HMOFs are not only rich in Ga-O units but also modified with abundant titanium ions, simply and effectively fulfilling the integration of IMAC and MOAC. Besides, the hydrophilicity introduced by modification of MOFs could also contribute to phosphoprotein enrichment through reducing nonspecific adsorption [26]. As expected, HMOFs exhibited high selectivity, large loading capacity and low limit of detection. Moreover, the comprehensively region-resolved phosphoproteome analysis of human lens was accomplished for the first time. The label-free quantification experiments and principal component analysis presented differential expression of phosphoproteins in three regions and disclosed the heterogeneity of phosphoproteome in human lens. This will be beneficial to the mechanism research on eye disease for better prevention, early screening and treatment.

HMOFs were prepared as illustrated in Scheme 1. To begin with, Fe_3O_4 nanoparticles with dense SiO_2 coating were generated according to previous work [27]. Then the formation of Ga-MiL-124 on outside surface was carried out through a hydrothermal reaction. Afterwards, extra Ti ions were introduced through the coordination between titanium ions and free carboxyl group of Ga-MiL-124 to obtain HMOFs. From transmission electron microscopy (TEM) images in Fig. S1 (Supporting information), the Fe_3O_4@SiO_2 nanoparticles exhibited a spherical morphology with an average particle diameter of 320 nm. MiL-124 coating could be seen in Fig. S1b with about 40 nm with comparison of Fe_3O_4@SiO_2, implying the successful immobilization of Ga-MiL-124 coatings on the surface of Fe_3O_4@SiO_2 substrates. Fig. 1a demonstrated that the final HMOFs nanoparticles had the similar shape of Fe_3O_4@SiO_2@MiL-124 (FSM) nanoparticles. Energy dispersive X-Ray (EDX) spectroscopy showed the existence of Ga and Ti elements, indicating the abundant binding sites of HMOFs towards phosphopeptides (Fig. S2 in Supporting information). The wide XRD patterns (Fig. 1b) showed that the strong peak at 7.69° and the weak peak at 15.52° of HMOFs and FSM were in good agreement with the diffraction patterns of simulated MiL-124, convincingly demonstrating the modification of MiL-124 with good crystallinity. The elemental composition and valence states were characterized by X-ray photoelectron spectroscopy (XPS), consistent with the results of EDX, suggesting the effective deposition of MiL-124 on the surface of Fe_3O_4@SiO_2 (Fig. 1c).

We also utilized FT-IR spectrum to characterize the structure of HMOFs. As seen in Fig. 1d, the wavenumber at 1547 cm^{-1} could be ascribed to the stretching vibration of C–O bonds of carboxyl and the peaks at 1450–1600 cm^{-1} belonged to the stretching vibration of benzene ring skeleton. Besides, the absorption peak of free carboxyl of 1,2,4-benzenetricarboxylic acid at 1711 cm^{-1} in Fig. S3 (Supporting information) was observed in FSM nanoparticles but absent in HMOFs, proving that Ti ions indeed coordinated with free carboxyl groups. Furthermore, as depicted in Fig. S4 (Supporting information), the FSM nanomaterials had a negative zeta potential of −2.05 mV and became positive after assembling with Ti ions through chelation, ultimately leading to the potential of HMOFs turned into 3.85 mV. The contact angle measurement demonstrated FSM nanoparticles possessed stonger hydrophilicity than Fe_3O_4@SiO_2 due to the modification of Ga-MiL-124, contributing to the better affinity of HMOFs towards phosphorylated peptides (Fig. S5 in Supporting information) [28]. All the above results implied the integration of MOAC and IMAC composed of abundant Ga and Ti metal sites would be favorable for the phosphoproteomics study.

It is reported that the nonspecific adsorption of acidic non-phosphorylated peptides could be restrained with suitable concentration of acetonitrile and TFA [28]. Therefore, we detected a series of concentrations on enrichment performance of HMOFs to

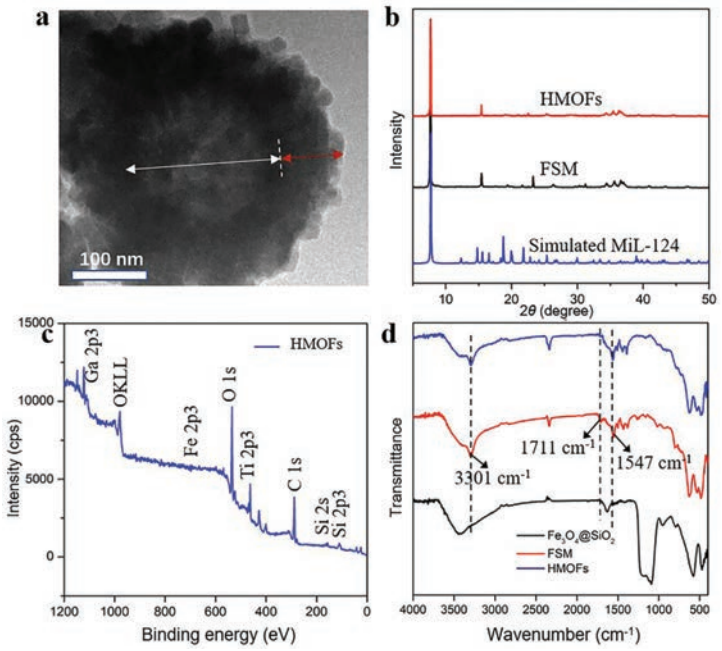

Fig. 1. (a) The TEM images of HMOFs. (b) The PXRD patterns of FSM, HMOFs and simulated MiL-124. (c) The XPS image of HMOFs. (d) The FT-IR spectra of Fe_3O_4@SiO_2, FSM and HMOFs. The white and red arrows in (a) represent Fe_3O_4@SiO_2 and MiL-124 layer, respectively.

reduce the interference as low as possible. 50% ACN and 2% TFA were considered as the optimized conditions of loading buffer based on the intensities of several standard phosphopeptides (Fig. S6 in Supporting information). As shown in Fig. 2, before treatment of HMOFs, there were several weak phosphopeptides in the mass spectra, while impurities with high intensities dominated the spectrum. In contrast, 13 mono-phosphorylated peptides and 6 multi-phosphorylated peptides with high signal to noise ratio (SNR) could be observed after enrichment with HMOFs. We also investigated the enrichment performance of FSM, where 11 and 5 peaks corresponding to mono- and multi-phosphorylated peptides were displayed with relatively weaker intensity in contrast with HMOFs. The detailed information could be seen in Table S1 (Supporting information). Both the increased number and improved intensity of identified phosphopeptides suggested the modification of titanium helped to strengthen the enrichment capacity of HMOFs. Then, we used the mixture of β-casein and BSA digests to explore the selectivity of HMOFs. 13 mono-phosphorylated peptides and 6 multi-phosphorylated peptides could be detected obviously in the mass spectra when the mass ratio of β-casein digests and BSA digests was 1:100, while the non-phosphopeptides with high SNR were dominant in the original mixture. Even when the mass ratio reached as high as 1:2000, there was still relatively pure MALDI-TOF MS spectrum with clean background, where 4 multi-phosphorylated peptides and 6 mono-phosphorylated peptides with high intensity and clear background were shown (Fig. S7 in Supporting information). The above results demonstrated that the HMOFs possessed excellent specificity and selectivity towards phosphopeptides, implying its good application in complicated biological samples.

Limit of detection (LOD) is another crucial parameter of nanomaterial employed in phosphopeptide detection due to the low abundance of targeted phosphopeptides. As illustrated in Fig. S8 (Supporting information), 7 mono-phosphorylated peptides and 4 multi-phosphorylated peptides were enriched after treatment with HMOFs when the concentration of β-casein digests was 1 fmol. In comparison, 4 and 4 peaks corresponding to mono- and multi-phosphorylated peptides with obvious background interfer-

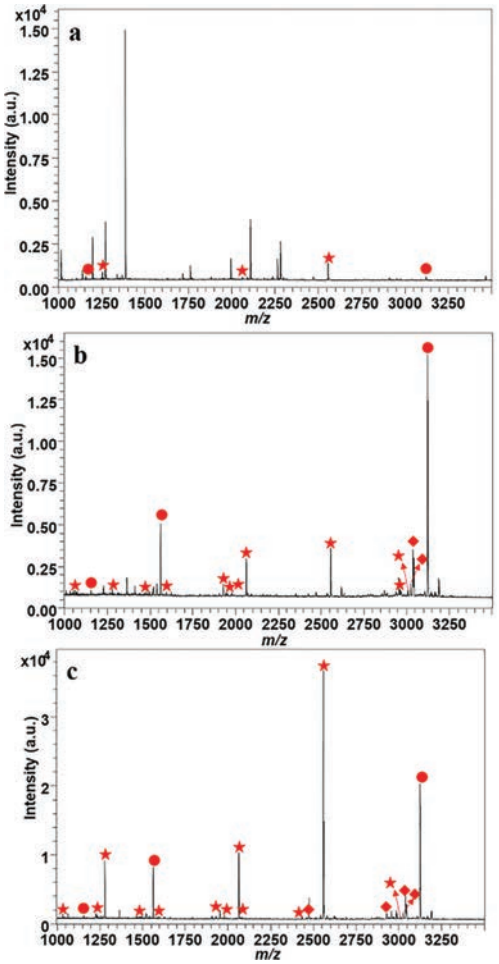

Fig. 2. The MALDI mass spectrum of identified phosphopeptides: before (a) and after treatment with FSM (b) and HMOFs (c) with 100 fmol/μL of β-casein. The identified mono- and multi-phosphorylated peptides and dephosphorylated peptides are marked with ⋆, ● and ♦, respectively.

ence could be identified after enrichment of FSM. Even when the concentration was as low as 0.1 fmol, there were still 2 mono-phosphorylated peptides and 2 multi-phosphorylated peptides shown in the Fig. S8, while only 1 multi-phosphorylated-peptide was detected in the mass spectrum with capture of FSM. The enhanced sensitivity might be attributed to the functionalization of Ti ion, which also manifested the robust identification ability of HMOFs nanomaterials towards low-abundant targeted molecules. Besides, the loading capacity of HMOFs was calculated to be 150 mg/g in accordance with the SNR of several standard phosphopeptides in the supernatant (Fig. S9 in Supporting information).

Human lens is a significant tissue in vision formation, whose malfunction inevitably induces age-related diseases, such as cataract, high myopia and glaucoma [29]. Region-resolved phosphoproteomics analysis of lens could be conductive to the understanding of lenticular etiology [30]. However, the global phosphoproteomics analysis with spatial information in lens still lacks. In consideration of the excellent properties of HMOFs, they were further applied in the spatial-scaled lenticular phosphopeptide enrichment. The bio-samples are from three regions of lens from three healthy people aged from 45 to 55 years old. As shown in Fig. S10 (Supporting information), a total of 1969 phosphorylated sites and 2293 phosphopeptides corresponding to 682 phosphoproteins were identified, containing 178 multi-phosphorylated peptides and 92 multi-phosphorylated proteins, which has been the broadest lenticular phosphoproteomics analysis by far. Interestingly, the Kyoto Encyclopedia of Genes and Genomes (KEGG) pathway analysis demonstrated that the identified phosphoproteins participated in the glycolysis/gluconeogenesis, which ranked the third most abundant enrichment pathway, implying the potential interplay between phosphorylation and glycosylation (Fig. S11 in Supporting information) [31]. The correlation between lenticular phosphoproteins and glycoproteins needs to be further explored.

Then, great attentions have been paid to the phosphproteome in different regions, aiming to excavate valuable and discrepant biological knowledge of capsule, cortex and nucleus. To begin with, the amount of identified phosphopeptides, phosphosites and phosphoproteins were given in Fig. 3a. In three biological complicates, we first found that the capsules owned the most abundant phosphorylation modification with 1530 phosphopeptides and 1334 phosphosites corresponding to 564 phosphoproteins. Cortex took the second place, in which 1149 phosphopeptides and 1160 phosphosites corresponding to 316 phosphoproteins were identified, while 621 phosphopeptides and 517 phosphosites corresponding to 205 phosphoproteins could been enriched in lenticular nucleus. The detailed information could be seen in Fig. S12 and Table S2 (Supporting information). The GO analysis of whole identified phosphoproteins in different regions was performed in Fig. S13 (Supporting information), giving the differences and similarities in capsule, nucleus and cortex. Thereinto, there were more identified phosphoproteins in capsule participating in cytoskeleton organization corresponding to more situations at cytoskeleton and actin cytoskeleton. We speculated that it would be ascribed to the accommodation function of lens capsule [32]. Intriguingly, most of the phosphoproteins in three regions were preferentially located at extracellular exosomes, which needed to be further studied. Principal component analysis was conducted to get a general view of lenticular phosphoproteome, each region separated evidently, manifesting the heterogeneity among capsule, cortex and nucleus (Fig. 3b).

Next, to figure out and refine the specific difference in spatial scale, we plotted heatmap of phosphoproteins through label-free quantification. As illuminated in Fig. 3c, the three regions could be distinguished visibly due to the disparate abundance of phosphoproteins, corroborating the heterogeneous features in three lens regions. Thereinto, β-crystallin obtained the least abundance in ocular capsule compared with nucleus and cortex, which would lead to cataracts by its mutation [33]. Besides, the fibrillin-1 as a known phosphoprotein was region-specifically distributed in the lens capsule, the malfunction of which might induce Marfan syndrome and concomitant symptoms, such as cataract or lens dislocation [34,35]. The preferential expressed phosphoproteins were involved in cytoskeleton organization, metabolic process and lens development in camera-type eye in capsule, cortex and nucleus, respectively. In addition, the heatmap of phosphosites across different regions was displayed in Fig. S14 (Supporting information) which provided more concrete phosphorylation and filtered 257 differentially expressed phosphosites. For instance, the phosphorylation of T4, T148 in α-crystallin A chain and S21, S76, T170 in α-crystallin B chain were enriched more abundantly in cortex and nucleus contrasted with capsule, which made consanguineous impacts on its molecular chaperone function [36]. Moreover, cortex and nucleus owned more phosphorylation status of S63 and S211 in heat shock protein 90 (HSP90) which went through the epidermal growth factor receptor (EGFR) pathway and acted as a novel therapy targeting for posterior capsule opacification [37]. On account of the differential expressed phosphoproteins and phosphosites in spatial dimension, it might be beneficial to screening potential biomarkers for precision medicine.

In brief, we developed a bifunctional nanoprobe with extremely low limit of detection, high sensitivity and outstanding selectivity, based on which a region-resolved of human lens for the first time was obtained. The label-free quantification and principle component analysis illuminated that the phosphorylation contents of three regions have significant differences. The preferential expressed phosphoproteins in capsule, cortex and nucleus were involved in cytoskeleton organization, metabolic process and lens de-

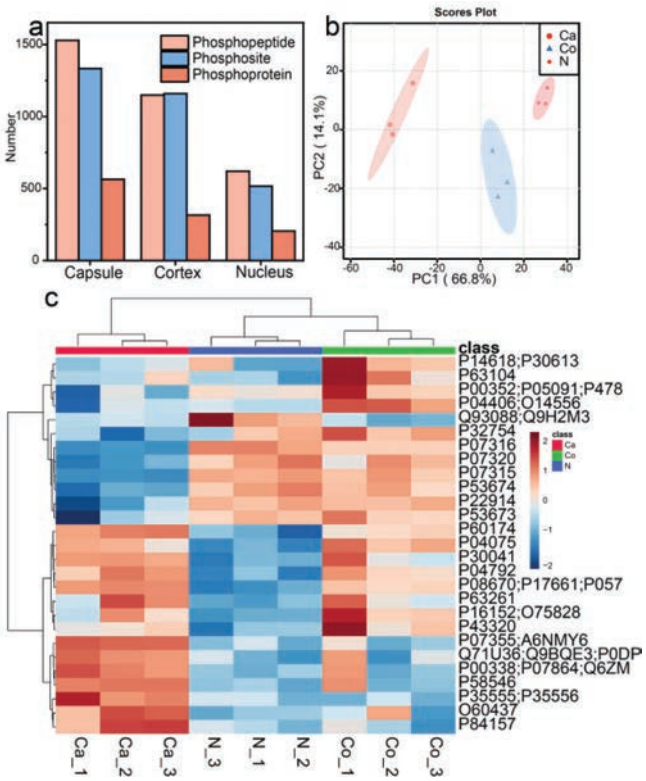

Fig. 3. (a) The enriched phosphopeptides, phosphoproteins and phosphosites in three regions. (b) The principle component analysis (PCA) of three lenticular regions. (c) Heatmap of differentially expressed phosphorylated proteins across different regions. Ca, Co and N represent capsule, cortex and nucleus, respectively.

velopment in camera-type eye. Besides, the phosphorylation heterogeneity helped to filtrate the potential biomarker for precise medicine. We provided a phosphorylation distribution overview of human lens for the first time and it will open a new avenue for the studies of lenticular diseases in a spatial scale.

Declaration of competing interest

The authors declare no conflict of interest.

Acknowledgments

This work was financially supported by National Key R&D Program of China (No. 2018YFA0507501), the National Natural Science Foundation of China (Nos. 22074019, 21425518 and 22004017), and Shanghai Sailing Program (No. 20YF1405300).

Supplementary materials

Supplementary material associated with this article can be found, in the online version, at doi:10.1016/j.cclet.2022.07.059.

References

[1] Y.C. Liu, M. Wilkins, T. Kim, B. Malyugin, J.S. Mehta, Lancet 390 (2017) 600–612.
[2] K.W. Roskamp, C.N. Paulson, W.D. Brubaker, R.W. Martin, Acc. Chem. Res. 53 (2020) 863–874.
[3] S.R. Flaxman, R.R.A. Bourne, S. Resnikoff, et al., Lancet Glob. Health 5 (2017) e1221–e1234.
[4] J.D. Steinmetz, R.R.A. Bourne, P.S. Briant, et al., Lancet Glob. Health 9 (2021) E144–E160.
[5] L. Zhao, X.J. Chen, J. Zhu, et al., Nature 523 (2015) 607–611.
[6] Z. Wang, J. Han, L.L. David, K.L. Schey, Investig. Ophthalmol Vis. Sci. 54 (2013) 1135–1143.
[7] J.A. Carver, H. Ecroyd, R.J.W. Truscott, D.C. Thorn, C. Holt, Acc. Chem. Res. 51 (2018) 745–752.
[8] A.C. Grey, K.L. Schey, Investig. Ophthalmol Vis. Sci. 50 (2009) 4319–4329.
[9] S.W. Bae, J.I. Kim, I. Cuot, et al., Anal. Sci. 33 (2017) 1381–1386.
[10] H.T. Wu, C.C. Hsu, C.F. Tsai, et al., Proteomics 11 (2011) 2639–2653.
[11] L. Zhang, Z. Liang, L. Zhang, Y. Zhang, S. Shao, Anal. Chim. Acta 900 (2015) 46–55.
[12] H.Y. Zhong, X. Xiao, S. Zheng, et al., Nat. Commun. 4 (2013) 1656.
[13] N.R. Sun, H.L. Yu, H. Wu, X.Z. Shen, C.H. Deng, TRAC-Trends Anal. Chem. 135 (2021) 116168.
[14] D.S. Yang, X.Y. Ding, H.P. Min, et al., J. Chromatogr. A 1505 (2017) 56–62.
[15] Z.Y. Sun, K.L. Hamilton, K.F. Reardon, Anal. Biochem. 445 (2014) 30–37.
[16] J.W. Wang, Z.D. Wang, N.R. Sun, C.H. Deng, Microchim. Acta 186 (2019) 9.
[17] J. Xiao, S.S. Yang, J.X. Wu, et al., Anal. Chem. 91 (2019) 9093–9101.
[18] J.Q. Zhou, Y.L. Liang, X.W. He, L.X. Chen, Y.K. Zhang, ACS Sustain. Chem. Eng. 5 (2017) 11413–11421.
[19] Y.N. Pan, C.H. Zhang, R.L. Xiao, L.Y. Zhang, W.B. Zhang, Anal. Chim. Acta 1158 (2021) 338412.
[20] Y.L. Wu, H.L. Chen, Y.J. Chen, N.A.R. Sun, C.H. Deng, Sci. China Chem. 65 (2022) 650–677.
[21] Y. Wang, Q. Ye, M.H. Yu, X.J. Zhang, C.H. Deng, Chin. Chem. Lett. 31 (2020) 1843–1846.
[22] S. Zhang, X. Pei, H.L. Gao, S. Chen, J. Wang, Chin. Chem. Lett. 31 (2020) 1060–1070.
[23] C.L. Pu, H.L. Zhao, Q.Y. Gu, Y. Zheng, M.B. Lan, Microchim. Acta 187 (2020) 568.
[24] Y.T. He, Q. Zheng, Z. Lin, Microchim. Acta 188 (2021) 150.
[25] J.X. Peng, H.Y. Zhang, X. Li, et al., ACS Appl. Mater. Interfaces 8 (2016) 35012–35020.
[26] H. Zhou, M. Ye, J. Dong, et al., S. Mohammed, Nat. Protoc. 8 (2013) 461–480.
[27] Y.L. Wu, N.R. Sun, C.H. Deng, ACS Appl. Mater. Interfaces 8 (2020) 9814–9823.
[28] Z. Wang, J. Wang, N. Sun, C. Deng, Anal. Chim. Acta 1067 (2019) 1–10.
[29] P.J. Foster, Y. Jiang, Eye 28 (2014) 202–208.
[30] Z. Wang, J. Han, K.L. Schey, J. Proteome Res. 7 (2008) 2696–2702.
[31] Z. Wang, N.D. Udeshi, C. Slawson, et al., Sci. Signal. 3 (2010) ra2.
[32] S. Krag, T.T. Andreassen, Prog. Retin Eye Res. 22 (2003) 749–767.
[33] Z. Ma, W. Yao, C.C. Chan, et al., Biochim. Biophys. Acta 1862 (2016) 1214–1227.
[34] W. Jones, J. Rodriguez, S. Bassnett, Dis. Model Mech. 12 (2019) dmm037283.
[35] J. DeDreu, J.L. Walker, A.S. Menko, Matrix Biol. 96 (2021) 18–46.
[36] E. Thornell, A. Aquilina, Cell Mol. Life Sci. 72 (2015) 4127–4137.
[37] J. Li, W. Xue, X. Wang, et al., Exp. Eye Res. 189 (2019) 107821.